Solid State Ionics 420 (2025) 116786

Contents lists available at ScienceDirect

Solid State Ionics

journal homepage: www.elsevier.com/locate/ssi

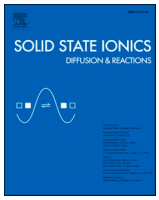

First-principles study on a lithium fluorooxoborate solid ion conductor

Shaohui Ding [a], Jian Sun [a], Daquan Yang [a,*], Huican Mao [b,*]

[a] State Key Laboratory of Information Photonics and Optical Communications, and School of Information and Communication Engineering, Beijing University of Posts and Telecommunications, Beijing 100876, China

[b] Department of Energy Storage Science and Engineering, School of Metallurgical and Ecological Engineering, University of Science and Technology Beijing, Beijing 100083, China

A B S T R A C T

Solid-state lithium-ion batteries have garnered significant interest due to their enhanced safety and superior energy density. A key component within solid-state batteries is the solid electrolyte, which plays a vital role in the battery's performance. In this work, we delve into the electronic structures and ionic diffusion characteristics of lithium fluorooxoborate, $Li_2B_3O_4F_3$ (LBOF), as a potential solid electrolyte material by First-principles calculations. The calculations indicate that the limited connectivity of low-energy barrier (0.08 eV) ion migration pathways, combined with significant vacancy formation energy (~6.0 eV), results in the poor ionic conductivity in crystalline LBOF. Additionally, we explore an effective strategy to reduce the hopping distance for lithium ions by inducing local disorder in LBOF, thereby enhancing its ionic conductivity properties. Our insights have shed new light on the strategies to alter ionic conductivity in the field of solid electrolyte materials, thus accelerating the innovation of solid-state battery technology.

1. Introduction

Electrochemical energy storage systems, such as lithium-ion batteries, are renowned for their efficiency and reliability in storing electrical energy, making them indispensable for portable electronics and electric vehicles [1–4]. However, the flammable nature of the organic liquid electrolytes used in current commercial lithium-ion batteries poses a significant fire hazard during incidents of overcharging or mishandling, which is particularly concerning in large-scale deployments [5,6]. Developing solid-state battery (SSB) technology by substituting solid electrolytes (SEs) for liquid ones has been a longstanding approach to mitigate safety risks associated with flammable components [7–11]. Yet, the advancement of solid-state batteries is heavily dependent on the availability of solid electrolytes that can support rapid ion transport.

For several decades, scientists have been striving to enhance the ionic conductivity of inorganic solid electrolytes with various improvement strategies, including the discovery of new materials, doping and substitution, grain boundary engineering, composite electrolytes, and so on [12–15]. Employing these enhancement tactics, significant strides have been achieved in the realm of ionic conductivity. For example, Mitsui et al. reported the identification of novel SE $Li_{10}GeP_2S_{12}$ with exceptional ionic conductivity ~10^{-2} S/cm at room temperature, which represents a major breakthrough [16]. In 2024, Sun et al. balanced Li-ion concentration and generated vacancies to enable an optimized ionic conductivity of 1.04 × 10^{-3} S/cm for Li_4YI_7, by manipulating the doping defects in the iodide structure [17]. Besides these strategies discussed, recent findings reveal that amorphous constituents within SEs can also substantially boost their ionic conductivity. Sun et al. reported the presence of amorphous component could significantly reduce the energy barriers for Li-ion transport, thus resulting in an enhanced ionic conductivity of 1.35 × 10^{-3} S/cm for amorphous $Li_3ZrCl_4O_{1.5}$ [18]. They also developed a glassy/crystalline composite electrolyte to effectively mitigate Li intrusion, achieving high ionic conductivity of 2.21 × 10^{-3} S/cm in $75Li_2S$-$25P_2S_5$ glass [19]. In addition, Hu et al. reported a class of viscoelastic inorganic glass to serve as SE, possessing high ionic conductivity ~1.0 × 10^{-3} S/cm for both Li and Na ions in Li/$NaAlCl_{2.5}O_{0.75}$ system [20]. These findings have shown that the incorporation of amorphous components within SEs is an effective strategy for improving the transport of alkali metal ions.

In 2012, Jansen et al. synthesized a new lithium fluorooxoborate, $Li_2B_3O_4F_3$ (LBOF), which is crystallized in the $P2_12_12_1$ space group. The measured impedance spectroscopy indicates it has the highest Li-ion conductivity among the hitherto know lithium fluorooxoborates, with conductivity of 1.8 × 10^{-8} S/cm at 523 K, exhibiting typical characteristics of ionic conductors [21]. The DFT calculated band structure displays the property of insulating material with wide band gaps 6–7 eV [22]. At present, no theoretical research has been conducted to explore the lithium-ion transport properties of LBOF, including the transport mechanism, pathways, and activation energy for lithium ions. Consequently, it is imperative to conduct further theory calculations on the

* Corresponding authors.
E-mail addresses: ydq@bupt.edu.cn (D. Yang), hcmao@ustb.edu.cn (H. Mao).

https://doi.org/10.1016/j.ssi.2025.116786
Received 16 October 2024; Received in revised form 8 January 2025; Accepted 16 January 2025
Available online 21 January 2025

ionic transport properties of LBOF, as well as to investigate potential modification strategies.

In this work, we combine bond valence (BV) and density functional theory (DFT) calculations to explore the electronic structures, ionic transport properties and potential modification strategies for LBOF. Our calculations clarify the factors contributing to the poor ionic conductivity in crystalline LBOF. Of particular significance, our molecular dynamics simulations (MD) have found that the amorphous LBOF has a decreased Li ion hopping distance, thereby boosting the conductivity of Li ions.

1.1. Computational details

In this work, all calculations were conducted utilizing the crystal structure of LBOF, which is crystallized in the acentric orthorhombic space group $P2_12_12_1$ with the cell parameters a = 4.8915, b = 8.734 and c = 12.301 Å [21]. We carried out the DFT calculations using Vienna Ab-initio Simulation Package (VASP) code based on density functional theory [23,24]. In DFT calculations, the exchange-correlation potential is characterized by employing the Perdew-Burke-Ernzerhof (PBE) [25] form of the generalized gradient approximation (GGA) [26]. For calculations of electronic structures, we employed 5 × 3 × 2 k-mesh grid and energy cutoff of 500 eV. All ions and cells were fully relaxed until the total energies and ionic forces were less than 10^{-5} eV and 0.01 eV·Å^{-1}, respectively. The electronic band structures and density of states were calculated using GGA and Heyd-Scuseria-Erznerhof (HSE) hybrid functional respectively [27], implemented in the DS-PAW software (2023 A) within the Device Studio program [28]. We used the quasiempirical bond-valence method [29,30] to obtain the possible ionic transportation channels of LBOF. Based on the favorite Li-ion migration channel, the migration barrier of Li ion was acquired by the climbing image nudged elastic band (CI-NEB) method [31] as implemented in VASP based on 2 × 1 × 1 supercell with 96 atoms.

Furthermore, the Ab Initio Molecular Dynamics (AIMD) simulations were performed on 2 × 1 × 1 supercell at different temperatures *T* (700 K ~ 1100 K), lasting for 55,000 steps with a time step of 1 fs. The first 6 ps are used to equilibrate the system at the temperature, and the mean-squared displacement (MSD) was calculated from the last 50 ps. To acquire the amorphous LBOF configuration, the supercell was initially melted and equilibrated at a high temperature of 3000 K, and quenched down to 300 K at the cooling rate of 1.0 × 10^{14} K/s to achieve a well-relaxed state. After obtaining the amorphous structure, AIMD simulations were performed at temperatures ranging from 700 to 1100 K for 55 ps to study the ion transport properties and structural changes of LBOF.

2. Results and discussion

2.1. Crystal structure

$Li_2B_3O_4F_3$ is crystallized in the orthorhombic crystal system, belonging to the $P2_12_12_1$ space group. As shown in Fig. 1a, the framework of the crystal structure is composed of $[B_3O_4F_3]^{2-}$ chains that extend along the *b*-axis, which are bonded to each other by a bridging oxygen atom. In Fig. 1b, the $[B_3O_4F_3]^{2-}$ chain unit, indicated by the green dashed circle in Fig. 1a, is specifically illustrated. In this configuration, the threefold ring-B atom (B3), which is bonded to two O atoms within the ring and one O atom that serves as a bridge, is connected to a fourfold coordinated B atom (B1). This B1 atom is linked to two ring-O atoms, one bridging O atom and one adjacent F atom. On the other hand, the third ring-B-atom (B2) is associated with two ring-O atoms and two terminal F atoms [21]. Noting that the chain-like B-O-B framework in LBOF bears a strong resemblance to the Al-O-Al network structure present within viscoelastic inorganic glass $Li/NaAlCl_{2.5}O_{0.75}$ [20], which may provide continuous pathways that facilitate the migration of Li^+/Na^+ ions, potentially enhancing the ionic conductivity of the electrolyte.

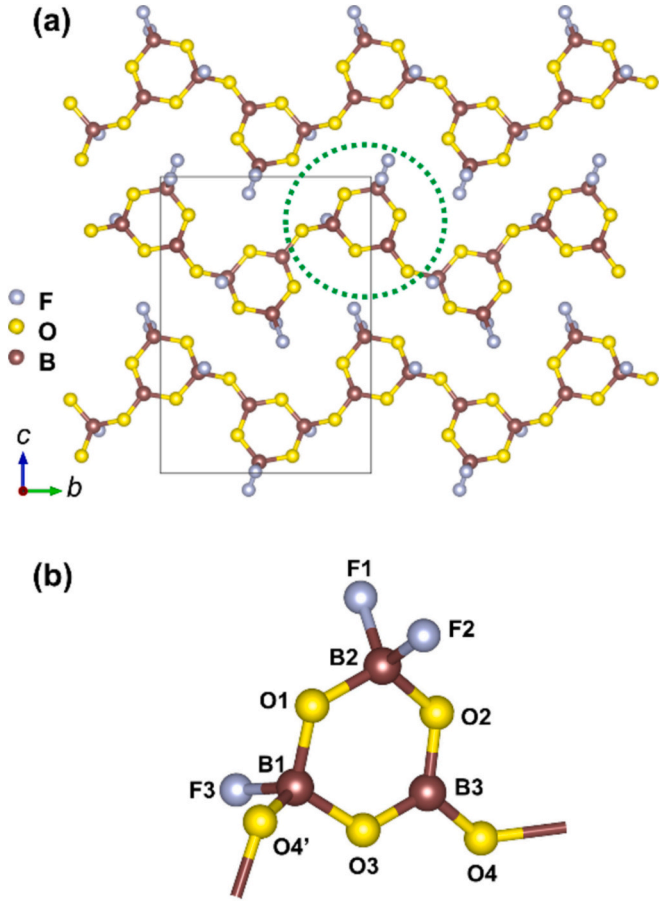

Fig. 1. (a) The $[B_3O_4F_3]^{2-}$ chain structure of LBOF. (b) The enlarged $[B_3O_4F_3]^{2-}$ chain unit (marked in green dashed circle in Fig. 1a). The fundamental building block $[B_3O_4F_3]^{2-}$ comprises one trigonal planar BO_3 unit, one tetrahedral BO_2F_2 unit, and one tetrahedral BO_3F unit. The grey balls represent F, the yellow balls represent O, and the brown balls represent B. (For interpretation of the references to colour in this figure legend, the reader is referred to the web version of this article.)

2.2. Electronic structure

DFT calculations were conducted to estimate the electronic band structure and density of states (DOS) of LBOF. As shown in Figs.2a, b, the calculated results suggest that LBOF has a substantial band gap of approximately 6.3 eV, which is in accordance with the local density approximation (LDA) calculation yielding a range of 6 to 7 eV [22]. Since GGA and LDA tend to underestimate the band gap, the HSE06 hybrid functional was also used to obtain more accurate band gap and electronic structures. As shown in Fig. 2, the electronic structures derived from the GGA and HSE methods are largely comparable, except for the difference in the magnitude of the band gap. The band gap of 8.4 eV obtained from the HSE method (Figs.2c, d) is 2.1 eV larger than the band gap of 6.3 eV obtained from the GGA method (Figs.2a, b). The top valence bands mainly derive from oxygen and fluorine, whereas the bottom conduction bands are predominantly contributed from boron and oxygen. For LBOF, the substantial band gap guarantees the first step to be a potential ionic conductor exhibiting rapid ionic conductivity.

2.3. Ionic transport mechanism

Now, we turn to the lithium-ion diffusion characteristics of LBOF by combining bond valence (BV) method and nudged elastic band (NEB) technique. First, we utilize a quasi-empirical BV method to identify potential channels for ion transport. As shown in Fig. 3a, the isosurfaces

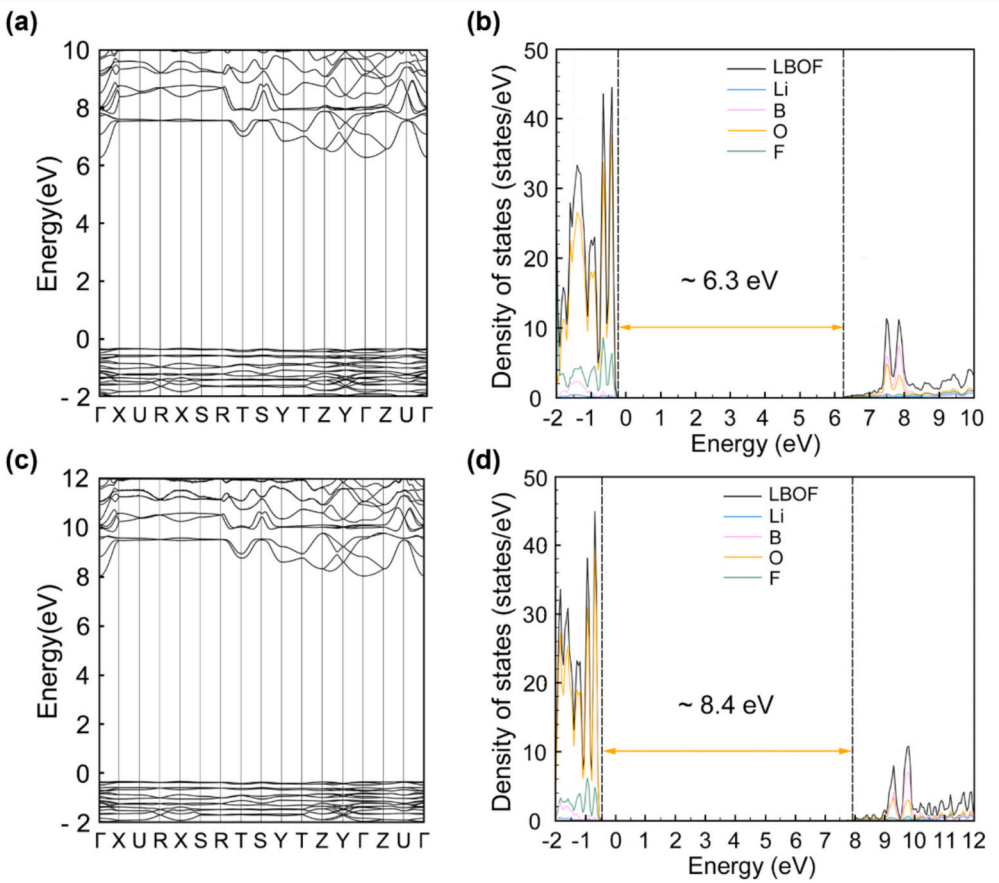

Fig. 2. The (a) electronic band structure and (b) density of states of LBOF obtained by GGA method. The (c) electronic band structure and (d) density of states of LBOF obtained by HSE06 method.

of potential energy (at 0.25 eV), indicated by the light purple belts, are treated as a pervasive network that supports the movement of lithium ions. The favorite Li^+ ion migration pathway suggests that one-dimensional transportation behavior is anticipated for this compound, with the ion conduction pathway extending in the direction of the a-axis within the crystal lattice.

To decipher the kinetic features unveiled by the BV approach, we perform NEB calculations to model a vacancy-mediated hopping process, aiming to ascertain the activation energy associated with the Li^+ ion hopping pathway. We have determined a segment of the periodic migration path, including the routes from P1 to P2 as illustrated in Fig. 3b. The calculations reveal that LBOF exhibits a migration barrier of 0.08 eV, substantially lower than those observed in general $Li_{10}GeP_2S_{12}$ (LGPS, ~0.24 eV) [16] and $Li_7La_3Zr_2O_{12}$ (LLZO, ~0.31 eV) [32] fast ionic conductor. This finding strongly suggests that LBOF may possess an exceptionally high lithium-ion conductivity.

However, the experimentally measured Li^+ ionic conductivity of LBOF is 1.8×10^{-8} S/cm at 523 K [22], indicating that LBOF is a poor Li-ion conductor. To investigate the discrepancy between experiments and calculations, we have meticulously examined the BV calculation results. As shown in Fig. 3a (isosurface level = 0.25 eV) and Fig. 3c (isosurface level = 1.25 eV), we find that these Li ions can be divided into two groups. The Li ions on the continuous connected paths P1-P2 can be labeled as Li1 and represented in light green, whereas the others can be labeled as Li2 and represented in dark green. We note that the migration path of Li2 ions becomes continuous at an isosurface level 1.25 eV, which suggests that the energy barrier for Li2 ions (~1.25 eV) is significantly greater than that for Li1 ions (~0.25 eV).

To attain superior ionic conductivity, it is imperative to possess both a reduced activation energy and an abundant presence of mobile charge carriers, such as vacancies or interstitials [33]. We have evaluated the formation energy of Li vacancies in LBOF. The calculated Li vacancy formation energies for Li1 and Li2 are 5.64 eV and 6.08 eV respectively, which are greater than those calculated in fast ion conductors such as LGPS (3.03 eV) and LLZO (3.69 eV). In general, we attribute the low ionic conductivity experimentally observed in crystalline LBOF to two primary factors: the relatively high energy required to form Li1, Li2 vacancies and the significant energy barrier associated with the pathway of Li2 ions.

2.4. *Strategies for improving ionic conductivity*

Prior studies have demonstrated that solid electrolytes in a homogeneously or heterogeneously disordered state, typically exhibit significantly increased ionic diffusivity compared to their microcrystalline or single crystalline counterparts [18–20]. Therefore, we intend to incorporate the amorphous phase into the LBOF electrolyte for enhancing its ionic transport properties. We first obtain the amorphous structure of LBOF by completely melting its crystalline structure at a high temperature of 3000 K followed by rapidly cooling down to ambient temperature. By examining both the crystalline and amorphous structures of LBOF in Figs.4a, b, it is observed that the amorphous structures lack any long-range order, which is in stark contrast to the ordered arrangement seen in its crystalline counterpart. This disorder in amorphous material results in the formation of multiple distinct microstructural fragments within LBOF. In the amorphous structure, two shortest distances for Li^+ hopping are identified as 2.88 Å and 3.07 Å (Fig. 4d), which are smaller than the corresponding Li—Li distances of 3.11 Å and 3.40 Å in its crystal structure (Fig. 4c), consistent with the calculated radial distribution function g(r) in Fig. 4e.

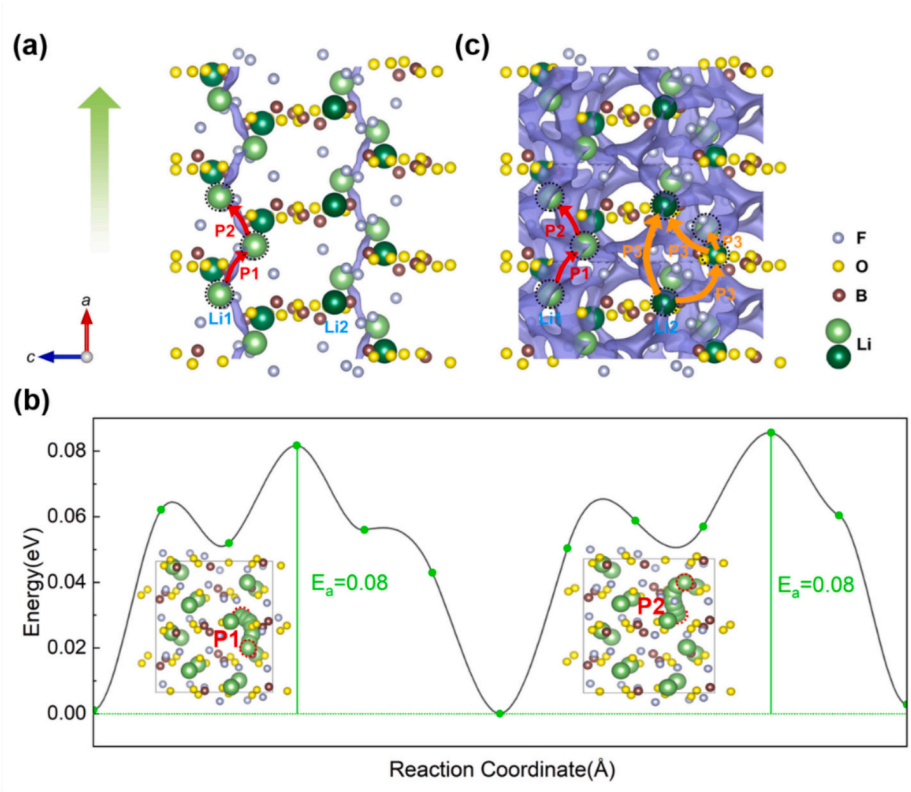

Fig. 3. The continuous Li^+ migration channels determined by BV method at isosurface level of (a) 0.25 eV and (c) 1.25 eV. (b) The energy barrier along migration pathways P1 and P2 by NEB method for LBOF.

For both crystalline and amorphous structures of LBOF, the AIMD simulations were carried out to quantify their Li^+ ionic conductivity. As shown in Figs.4f, g, the larger MSD values over the time interval $\Delta t \sim 50$ ps demonstrate that the amorphous structure exhibits higher slope compared to its crystalline counterpart. This is consistent with the distribution of Li atom positions during AIMD simulations at 700 K, as indicated by the bright-yellow points in Figs.4a, b. The Arrhenius equation is employed for linearly fitting log(D) against 1/T to derive the total activation energy and ionic conductivity. As shown in Fig. 4h, the conductivity of crystalline LBOF is 3.43×10^{-9} S/cm at 523 K, which is in agreement with the experimental result of 1.8×10^{-8} S/cm at 523 K. For amorphous LBOF, the extrapolated Li^+ conductivities are 6.49×10^{-4} S/cm at 300 K and 5.39×10^{-2} S/cm at 523 K, which is significantly enhanced compared to its crystalline phase. In addition, the estimated activation energies for crystalline and amorphous LBOF are 1.60 eV and 0.30 eV respectively. The room-temperature ionic conductivity and activation energy of amorphous LBOF are comparable to that of LLZO (0.31 eV, 3×10^{-4} S/cm) [32] and LGPS (0.24 eV, 9×10^{-3} S/cm) [34] at 300 K, which suggests that amorphous LBOF is highly promising as a good candidate for fast ionic conductor. The intrinsic presence of B-O-B chains, as well as the reduced Li—Li hopping distances, contributes to the enhanced ionic conductivity of LBOF in its amorphous state, which resembles the ionic conductivity mechanism characterized for viscoelastic inorganic glass electrolytes Li/NaAlCl$_{2.5}$O$_{0.75}$ [20].

2.5. *Electrochemical stabilities*

To delve into the electrochemical stability of crystalline LBOF, we have utilized DFT calculations and Materials Project database [35] to assess its electrochemical windows. As shown in Fig. 5, the predicted stability window is relatively wide with 1.87–4.45 V, which indicates LBOF has potential stability in electrochemical applications. The wide electrochemical window of LBOF can be mainly credited to its unique chemical composition and crystal structure, with the high electronegativity of F providing the material with excellent oxidative stability. Given its robustness at high voltage levels, LBOF is expected to be an essential component in the advancement of future all-solid-state battery technologies.

3. Conclusions

In conclusion, the first-principle calculations have revealed that LBOF possesses a substantial band gap of 8.406 eV, suggesting excellent electronic insulation. The calculations suggest that the poor ionic conductivity in crystalline LBOF is due to the restricted connectivity of ion migration pathways with low energy barriers of 0.08 eV and the substantial energy required for vacancy formation (approximately 6.0 eV). Moreover, we have identified an effective strategy to further enhance the ionic conductivity of LBOF through the introduction of local disorder, which offers a novel pathway to tailor the performance of solid electrolyte materials. These findings are expected to contribute significantly to the advancement of solid-state battery technology, offering a promising direction for future research and innovation in the field of energy storage.

CRediT authorship contribution statement

Shaohui Ding: Writing – original draft, Visualization, Data curation. **Jian Sun:** Writing – original draft, Investigation, Data curation. **Daquan Yang:** Supervision, Project administration. **Huican Mao:** Writing – review & editing, Project administration, Methodology, Funding acquisition, Formal analysis, Conceptualization.

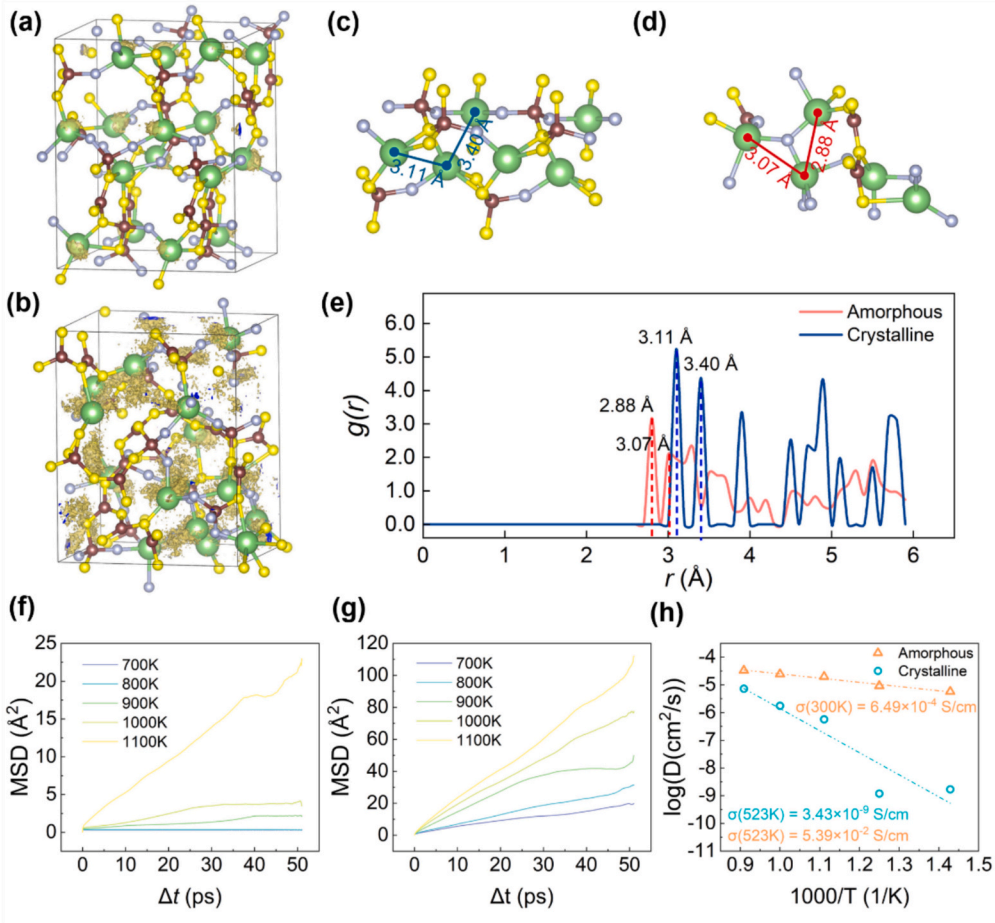

Fig. 4. The (a) crystalline and (b) amorphous structure of LBOF. The bright-yellow points represent the Li atom position distribution in LBOF during 50 ps. Microstructural fragments with the shortest Li^+ hopping distances of (c) crystalline and (d) amorphous LBOF. (e) The radial distribution function of Li—Li in crystalline and amorphous LBOF. The MSD of Li in (f) crystalline and (g) amorphous LBOF at temperatures ranging from 700 to 1100 K. (h) The calculated Arrhenius plots of Li^+ diffusivity D as a function of temperature T in crystalline LBOF and amorphous LBOF. The AIMD-estimated ionic conductivity of crystalline LBOF at 523 K and amorphous LBOF at 300 K and 523 K are displayed in panel. The green balls represent Li, the grey balls represent F, the yellow balls represent O, and the brown balls represent B. (For interpretation of the references to colour in this figure legend, the reader is referred to the web version of this article.)

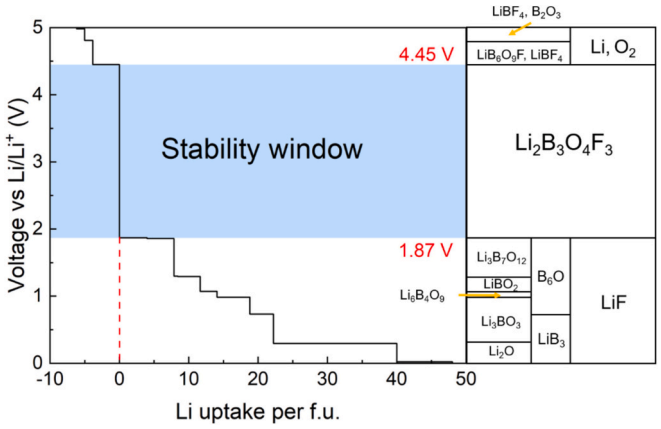

Fig. 5. The calculated voltage profile of crystalline LBOF upon lithiation and delithiation.

Declaration of competing interest

The authors declare that they have no known competing financial interests or personal relationships that could have appeared to influence the work reported in this paper.

Acknowledgments

This work was supported by the funding from the National Natural Science Foundation of China (grant no. 22303114). We gratefully acknowledge HZWTECH for providing computation facilities.

H. M. and D. Y. conceived the project. S. D. conducted theoretical calculations. S. D., H. M. wrote the paper. All authors discussed and contributed to the writing.

Data availability

Data will be made available on request.

References

[1] Y. Nishi, Lithium ion secondary batteries; past 10 years and the future, J. Power Sources 100 (2001) 101–106, https://doi.org/10.1016/S0378-7753(01)00887-4.
[2] M. Armand, J.-M. Tarascon, Building better batteries, Nature 451 (2008) 652–657, https://doi.org/10.1038/451652a.
[3] B. Dunn, H. Kamath, J.-M. Tarascon, Electrical energy storage for the grid: a battery of choices, Science 334 (2011) 928–935, https://doi.org/10.1126/science.1212741.
[4] Z.M. Ali, M. Calasan, F.H. Gandoman, F. Jurado, S.H.E.A. Aleem, Review of batteries reliability in electric vehicle and E-mobility applications, Ain Shams Eng. J. 15 (2024) 102442, https://doi.org/10.1016/j.asej.2023.102442.
[5] J.-M. Tarascon, M. Armand, Issues and challenges facing rechargeable lithium batteries, Nature 414 (2001) 359–367, https://doi.org/10.1038/35104644.

[6] B. Scrosati, J. Garche, Lithium batteries: status, prospects and future, J. Power Sources 195 (2010) 2419–2430, https://doi.org/10.1016/j.jpowsour.2009.11.048.
[7] Y.-S. Hu, Batteries: Getting solid, Nat. Energy 1 (2016) 16042, https://doi.org/10.1038/nenergy.2016.42.
[8] Q. Zhao, S. Stalin, C.-Z. Zhao, L.A. Archer, Designing solid-state electrolytes for safe, energy-dense batteries, Nat. Rev. Mater. 5 (2020) 229–252, https://doi.org/10.1038/s41578-019-0165-5.
[9] A. Manthiram, X. Yu, S. Wang, Lithium battery chemistries enabled by solid-state electrolytes, Nat. Rev. Mater. 2 (2017) 16103, https://doi.org/10.1038/natrevmats.2016.103.
[10] C. Sun, J. Liu, Y. Gong, D.P. Wilkinson, J. Zhang, Recent advances in all-solid-state rechargeable lithium batteries, Nano Energy 33 (2017) 363–386, https://doi.org/10.1016/j.nanoen.2017.01.028.
[11] S. Randau, D.A. Weber, O. Kötz, R. Koerver, P. Braun, A. Weber, E. Ivers-Tiffée, T. Adermann, J. Kulisch, W.G. Zeier, F.H. Richter, J. Janek, Benchmarking the performance of all-solid-state lithium batteries 5 (2020) 259–270, https://doi.org/10.1038/s41560-020-0565-1.
[12] Y. Kato, S. Hori, T. Saito, K. Suzuki, M. Hirayama, A. Mitsui, M. Yonemura, H. Iba, R. Kanno, High-power all-solid-state batteries using sulfide superionic conductors, Nat. Energy 1 (2016) 16030, https://doi.org/10.1038/nenergy.2016.30.
[13] F. Zheng, M. Kotobuki, S. Song, M.O. Lai, L. Lu, Review on solid electrolytes for all-solid-state lithium-ion batteries, J. Power Sources 389 (2018) 198–213, https://doi.org/10.1016/j.jpowsour.2018.04.022.
[14] Y. Zheng, Y. Yao, J. Ou, M. Li, D. Luo, H. Dou, Z. Li, K. Amine, A. Yu, Z. Chen, A review of composite solid-state electrolytes for lithium batteries: fundamentals, key materials and advanced structures, Chem. Soc. Rev. 49 (2020) 8790, https://doi.org/10.1039/D0CS00305K.
[15] B. He, F. Zhang, Y. Xin, C. Xu, X. Hu, X. Wu, Y. Yang, H. Tian, Halogen chemistry of solid electrolytes in all-solid-state batteries, Nat. Rev. Chem. 7 (2023) 826–842, https://doi.org/10.1038/s41570-023-00541-7.
[16] N. Kamaya, K. Homma, Y. Yamakawa, M. Hirayama, R. Kanno, M. Yonemura, T. Kamiyama, Y. Kato, S. Hama, K. Kawamoto, A. Mitsui, A lithium superionic conductor, Nat. Mater. 10 (2011) 682–686, https://doi.org/10.1038/nmat3066.
[17] S. Zhang, F. Zhao, H. Su, Y. Zhong, J. Liang, J. Chen, M.L. Zheng, L.Y. Chang, J. Fu, S.H. Alahakoon, Y. Hu, Y. Liu, Y. Huang, J. Tu, T.-K. Sham, X. Sun, Cubic iodide LixYI3+x superionic conductors through defect manipulation for all-solid-state Li batteries, Angew. Chem. Int. Ed. 63 (2024), https://doi.org/10.1002/anie.202316360 e202316360.
[18] S. Zhang, F. Zhao, L.-Y. Chang, Y.-C. Chuang, Z. Zhang, Y. Zhu, X. Hao, J. Fu, J. Chen, J. Luo, M. Li, Y. Gao, Y. Huang, T.-K. Sham, M.D. Gu, Y. Zhang, G. King, X. Sun, Amorphous oxyhalide matters for achieving lithium superionic conduction, J. Am. Chem. Soc. 146 (2024) 2977–2985, https://doi.org/10.1021/jacs.3c07343.
[19] H. Su, Y. Zhong, C. Wang, Y. Liu, Y. Hu, J. Li, M. Wang, L. Jiao, N. Zhou, B. Xiao, X. Wang, X. Sun, J. Tu, Deciphering the critical role of interstitial volume in glassy sulfide superionic conductors, Nat. Commun. 15 (2024) 2552, https://doi.org/10.1038/s41467-024-46798-4.
[20] T. Dai, S. Wu, Y. Lu, Y. Yang, Y. Liu, C. Chang, X. Rong, R. Xiao, J. Zhao, Y. Liu, W. Wang, L. Chen, Y.-S. Hu, Inorganic glass electrolytes with polymer-like viscoelasticity, Nat. Energy 8 (2023) 1221–1228, https://doi.org/10.1038/s41560-023-01356-y.
[21] T. Pilz, H. Nuss, M. Jansen, Li2B3O4F3, a new lithium-rich fluorooxoborate, J. Solid State Chem. 186 (2012) 104–108, https://doi.org/10.1016/j.jssc.2011.11.053.
[22] B. Andriyevsky, K. Doll, T. Pilz, M. Jansen, DFT-based ab initio study of electronic band structure and elastic properties of Li2B3O4F3 and Li2B6O9F2 crystals, J. Phys. Chem. Solid 74 (2013) 624–629, https://doi.org/10.1016/j.jpcs.2012.12.017.
[23] G. Kresse, J. Furthmüller, Efficient iterative schemes for ab initio total-energy calculations using a plane-wave basis set, Phys. Rev. B 54 (1996) 11169, https://doi.org/10.1103/PhysRevB.54.11169.
[24] G. Kresse, J. Furthmüller, Efficiency of ab-initio total energy calculations for metals and semiconductors using a plane-wave basis set, Comput. Mater. Sci. 6 (1996) 15–50, https://doi.org/10.1016/0927-0256(96)00008-0.
[25] J.P. Perdew, M. Ernzerhof, K. Burke, Rationale for mixing exact exchange with density functional approximations, J. Chem. Phys. 105 (1996) 9982–9985, https://doi.org/10.1063/1.472933.
[26] J.P. Perdew, K. Burke, M. Ernzerhof, Generalized gradient approximation made simple, Phys. Rev. Lett. 77 (1996) 3865–3868, https://doi.org/10.1103/PhysRevLett.77.3865.
[27] J. Heyd, G.E. Scuseria, Efficient hybrid density functional calculations in solids: assessment of the Heyd–Scuseria–Ernzerhof screened coulomb hybrid functional, J. Chem. Phys. 121 (2004) 1187–1192, https://doi.org/10.1063/1.1760074.
[28] P.E. Blöchl, Projector augmented-wave method, Phys. Rev. B 50 (1994) 17953–17979, https://doi.org/10.1103/PhysRevB.50.17953.
[29] R. Xiao, H. Li, L. Chen, High-throughput design and optimization of fast lithium ion conductors by the combination of bond-valence method and density functional theory, Sci. Rep. 5 (2015) 14227, https://doi.org/10.1038/srep14227.
[30] S. Adams, R.P. Rao, High power lithium ion battery materials by computational design, Phys. Status Solidi A 208 (2011) 1746–1753, https://doi.org/10.1002/pssa.201001116.
[31] G. Henkelman, H. Jónsson, Improved tangent estimate in the nudged elastic band method for finding minimum energy paths and saddle points, J. Chem. Phys. 113 (2000) 9978–9985, https://doi.org/10.1063/1.1323224.
[32] R. Murugan, V. Thangadurai, W. Weppner, Fast lithium ion conduction in garnet-type Li7La3Zr2O12, Angew. Chem. Int. Ed. 46 (2007) 7778–7781, https://doi.org/10.1002/anie.200701144.
[33] X. He, Y. Zhu, Y. Mo, Origin of fast ion diffusion in super-ionic conductors, Nat. Commun. 8 (2017) 15893, https://doi.org/10.1038/ncomms15893.
[34] Y. Mo, S.P. Ong, G. Ceder, First principles study of the Li10GeP2S12 lithium super ionic conductor material, Chem. Mater. 24 (2012) 15–17, https://doi.org/10.1021/cm203303y.
[35] A. Jain, S.P. Ong, G. Hautier, W. Chen, W.D. Richards, S. Dacek, S. Cholia, D. Gunter, D. Skinner, G. Ceder, K.A. Persson, Commentary: the materials project: a materials genome approach to accelerating materials innovation, APL Mater. 1 (2013) 011002, https://doi.org/10.1063/1.4812323.